Journal of Applied Sciences and Nanotechnology

Journal homepage: jasn.uotechnology.edu.iq

Structural Characteristics of Alumina Nanoparticles Synthesised by DC Reactive Sputtering Technique

[1]Noor E. Naji*, [2]Ali A. Aljubouri, [3]Raid A. Ismail

[1]Department of Medical and Industrial Materials Science, College of Applied Sciences, University of Technology-Iraq, Iraq
[2]Department of Laser Science and Technology, College of Applied Sciences, University of Technology-Iraq, Iraq
[3]College of Applied Sciences, University of Technology-Iraq, Iraq

A R T I C L E I N F O

Article history:
Received: January, 21, 2025
Accepted: June, 09, 2025
Available online: September, 10, 2025

Keywords:
Al_2O_3,
Nanoparticles,
DC Reactive sputtering,
Structural Characteristics

Corresponding Author:
Noor E. Naji
noor.e.naji@uotechnology.edu.iq

A B S T R A C T

In this work, Al_2O_3 nanoparticles were synthesized using the DC reactive sputtering technique. A highly pure aluminum target was sputtered within a gas mixture containing oxygen. The structural characteristics of the synthesized nanoparticles were introduced by X-ray diffraction (XRD), field-emission scanning electron microscopy (FE-SEM), energy-dispersive X-ray spectroscopy (EDX), and atomic force microscopy (AFM). An inter-electrode distance of 4 cm can describe the operation parameters, Ar: O_2 gas mixing ratio of 50:50, applied voltage of 1500 V and discharge current of 25 mA. The prepared samples showed a polycrystalline structure with an amorphous nature due to the formation of nanoparticles, which were approximately spherical with a minimum size of 21 nm and an average grain size of 40.7 nm. Some agglomerations were observed in the prepared samples. The elemental composition analysis revealed that the prepared material contains aluminum and oxygen with no traces of other elements. The stoichiometry and homogeneity of the prepared material were also shown. All functional groups corresponding to the vibrational modes of the Al_2O_3 molecule were confirmed. The energy band gap of the prepared nanomaterial was determined based on its absorption spectrum and measured to be 4.46 eV; this demonstrates a promising approach for producing highly pure metal oxide nanomaterial by the DC reactive sputtering technique.

https://doi.org/10.53293/jasn.2025.7575.1335, Department of Applied Sciences, University of Technology - Iraq.

1. Introduction

Alumina or aluminium oxide (Al_2O_3) is the most common ceramic employed for modern technologies and industries. This material has a high melting point, high electric resistivity, high oxidation resistance, high hardness, low thermal conductivity, and high abrasion resistance [1-7]. All these physical and chemical properties, with a refractive index of 1.7, made this oxide an excellent candidate for cutting tools, optoelectronic devices, diffusion, and thermal barriers [8-14].

Aluminium oxidation can produce several phases (α, δ, γ, η, θ, χ, and κ). Only the phase alpha (α) is stable and shows trigonal structure, while all other phases are metastable [15-18]. The phase alpha is formed at temperatures up to 650 °C. In contrast, annealing at higher temperatures can lead to the development of metastable phases depending on the composition and structure of the initial materials [19-22]. **Fig. 1** shows the chemical structure of alumina (Al_2O_3) [23].

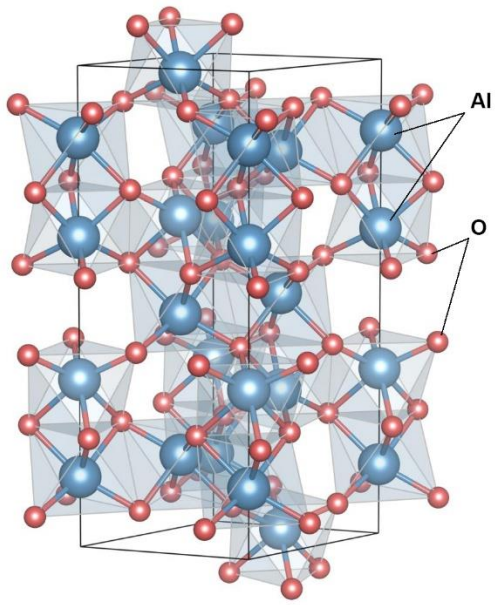

Figure 1: Crystal structure of alumina (Al_2O_3).

Many methods and techniques were used to prepare crystalline alumina, such as pulsed laser deposition (PLD) [24], ion-assisted deposition [25], chemical vapor deposition (CVD) [26], electron beam evaporation [27], spray pyrolysis [28], sol-gel [29], and magnetron sputtering [30, 31]. The latter technique (magnetron sputtering) was employed in the current study to deposit alumina (Al_2O_3) thin film on glass substrates.

By adjusting several operational parameters included in the reactive magnetron sputtering technique, precise control can be achieved over particle size, shape, structure, surface morphology, etc. [32-34]. Early studies on preparing alumina nanostructures using sputtering techniques include sputtering an alumina target by DC or RF discharge plasma [35]. Another approach proposed was sputtering a target of highly pure aluminum in the presence of oxygen [36]. Compared to other deposition methods and techniques, reactive sputtering ensures high-quality nanostructures, as the process occurs within a vacuum chamber and minimizes contaminants or residuals to the lowest level [37]. The Magnetron sputtering method, a large-scale, industry-ready physical vapor deposition technology, facilitates the development of unique coatings with efficacious therapeutic properties [38]. As a reproducible and scalable deposition technique, it allows for the directed fabrication or modification of the membrane by depositing a thin layer on a support layer [39]. It is an effective method for producing sputtered thin film materials based on metal oxide, metal nitride, alloys, carbon, and ceramic- based thin film, along with their properties and applicability in various fields [40]. Several chemical elements have been used to form multiple coating structures, including metastable solid solutions, binary and/or ternary phases, or mixtures thereof [41]. The capability to fabricate these nanostructures on various structures, including glass, silicon wafers, or flexible substrates, extends their range of applications, enabling the integration of nanostructured materials onto thin layers and allowing for the precise tuning of their physical and chemical properties of the materials [42]. In this work, Al_2O_3 nanoparticles are prepared by DC reactive sputtering and extracted as nanopowder using the freezing-assisted ultrasonic wave extraction method. The structural and spectroscopic characteristics of the synthesized nanopowder are introduced and analyzed.

2. Theoretical Part

2.1 Preparation Method

A DC reactive magnetron sputtering system was used to sputter an aluminum target with oxygen as a reactive gas to deposit thin aluminum oxide films on glass substrates. A highly pure (99.99%) aluminum target of 8 cm diameter and 1.5 mm thickness was cleaned, polished, and fixed on the cathode by a mount made of Teflon. Meanwhile, the glass substrate was thoroughly washed with ethanol and distilled water, dried, and fixed on the anode. The inter-electrode distance was set to 4 cm, which was selected according to the optimization of previous works to produce the most uniform plasma column. A gas mixture of 50:50 of argon and oxygen (Ar: O_2) was used, which also was selected according to the optimization of previous works to produce the most uniform thin films. The gas mixture pressure inside the sputtering chamber could be varied via a precise needle valve. The voltage applied to the discharge electrodes to produce plasma was 1500 V and 25 mA discharge current. The circulating water was used to cool the electrodes to prevent the effects of rising temperature. When the cooling system was turned off, the temperature gradually increased, reaching 300 °C. The experimental details of the sputtering system were previously reported [43, 44]. The deposition time was 90 min, which produces a film thickness of 150±10 nm. The film thickness was determined by laser interferometry using a laser diode of 630 nm and a focusing lens of 10 cm focal length. At the same time, the interference fringes were shown on a white screen.

The thin film material was extracted as nanopowder using the freezing-assisted ultrasonic waves extraction method [45, 46]. This technique exhibits the advantage of producing highly pure nanopowder without a trace of the substrate material on which the thin film is deposited.

2.2 Instruments and Devices

An AERIS PANalytical X-ray diffractometer (XRD) (Cu Kα source, 1.514 Å) was used to record the X-ray diffraction (XRD) patterns of the prepared samples within the diffraction angle range of 10°-80°. An FEI Inspect F50 field-emission scanning electron microscope (FE-SEM) was used to introduce the surface morphology and the energy-dispersive X-ray spectroscopy (EDS). NT-MDT Integra AFM instrument was used to study the surface roughness and topography of the prepared samples. The Fourier-transform infrared (FTIR) spectroscopy was applied on the obtained samples using a Perkin Elmer FTIR instrument. A Spectra Academy KMAC SV2100 UV-visible spectrophotometer was used to record the absorption spectra of the prepared samples in the UV-visible region.

The crystallite size and microstrain were determined by the following Eq. (1) and Eq.(2) [47]:

$$\boldsymbol{D = \frac{k\lambda}{\beta cos\theta}} \quad \textbf{(1)}$$

$$\boldsymbol{\varepsilon = \frac{\lambda}{\beta cos\theta}} \quad \textbf{(2)}$$

3. Experimental Procedure

3.1 XRD Results

Fig. 2 illustrate XRD pattern of the Al_2O_3 nanoparticles prepared in this work. There are six apparent diffraction peaks seen at diffraction angles (2θ) of 32.55°, 36.85°, 39.46°, 46.68°, 59.64°, and 66.98°, which correspond to the crystalline planes of (200), (311), (222), (400), (511), and (440), respectively, according to the JCPDS card no. 00-029-0063 [48]. However, the broadening of these peaks may confirm the formation of nanoparticles. In this pattern, no traces of elements and materials other than Al_2O_3 were found, which highlights the structural purity of these nanoparticles. This result demonstrates the advantage of the DC reactive sputtering technique in preparing this material. The parameters obtained from the XRD results are indicated in **Table 1**.

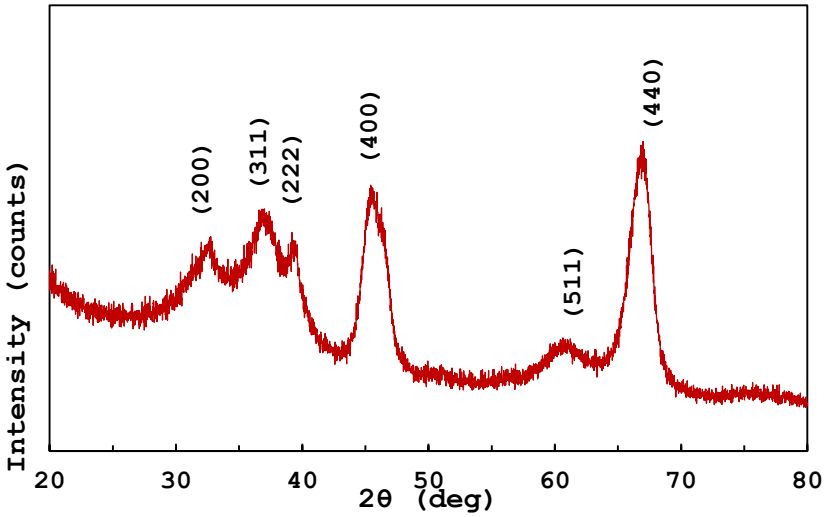

Figure 2: XRD pattern of prepared Al_2O_3 NPs.

Table 1: Analysis of the XRD and parameters of prepared Al_2O_3 NPs.

2θ (deg)	d-spacing (nm)	FWHM (rad)	Crystallite Size (nm)	Micro Strain (%)
32.8784	2.74802	0.8659	9.99	0.328447
36.8274	2.43721	0.8659	10.10	0.283299
39.1814	2.28164	0.4330	20.35	0.130092
45.4294	1.99121	0.9525	9.45	0.229374
60.6534	1.94405	0.9103	10.57	0.124129
66.8354	1.91186	0.8223	12.10	0.084784

3.2 FE-SEM Results

The FE-SEM image shown in **Fig. 3** analyzed the morphology of the prepared sample. A minimum particle size of about 21 nm and an average particle size ranging from 25 to 35 nm can be determined with approximately spherical-shaped and uniformly distributed particles. However, some agglomerated particles smaller than 500 nm can be seen. These agglomerations are mainly formed due to van der Waals attractive forces due to the high surface area available on the substrate on which the alumina films are deposited [32].

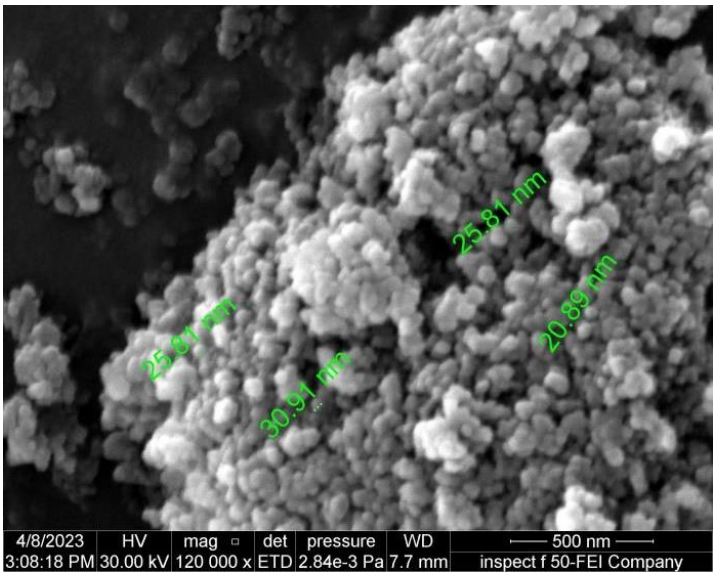

Figure 3: FE-SEM image of prepared Al_2O_3 NPs.

3.3 EDX Results

Fig. 4 presents the EDX spectrum and the elemental composition of the Al_2O_3 nanoparticles prepared in this work. The spectrum contains peaks belonging to aluminum and oxygen with an atomic ratio (Al/O) of 0.54, which is deviated by ~19% from the typical value (0.666). Similarly, the weight ratio determined from **Fig. 5** is 0.91, showing a 19% deviation from the usual value of 1.1243. These results may reveal the stoichiometry of the prepared compound. The presence of carbon (C) in the EDX spectrum and elemental composition is attributed to mounting the Al_2O_3 sample using a carbon-based adhesive material. These findings further suggest that the produced nanoparticles have excellent structural purity, which is related to the benefit of the DC reactive sputtering method [44].

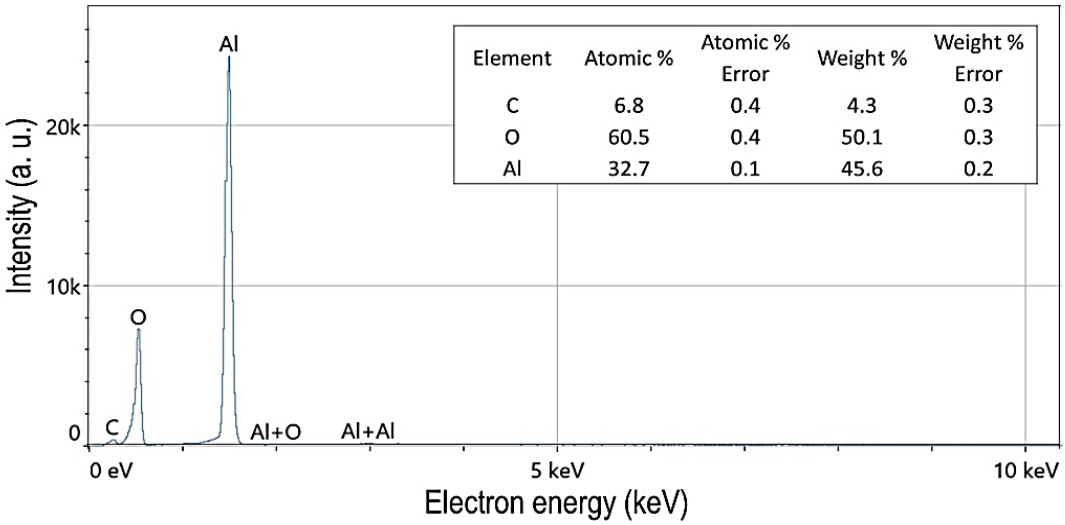

Figure 4: EDX result and elemental composition of the prepared Al_2O_3 NPs.

Fig. 5 presents the elemental mapping of the prepared Al_2O_3 nanoparticles, which shows the homogeneous distribution of Al and O atoms in the prepared sample. Such homogeneity might be due to the homogeneous deposition of Al_2O_3 film by the DC reactive sputtering technique, which tends to cover the substrate surface evenly with the prepared material [43].

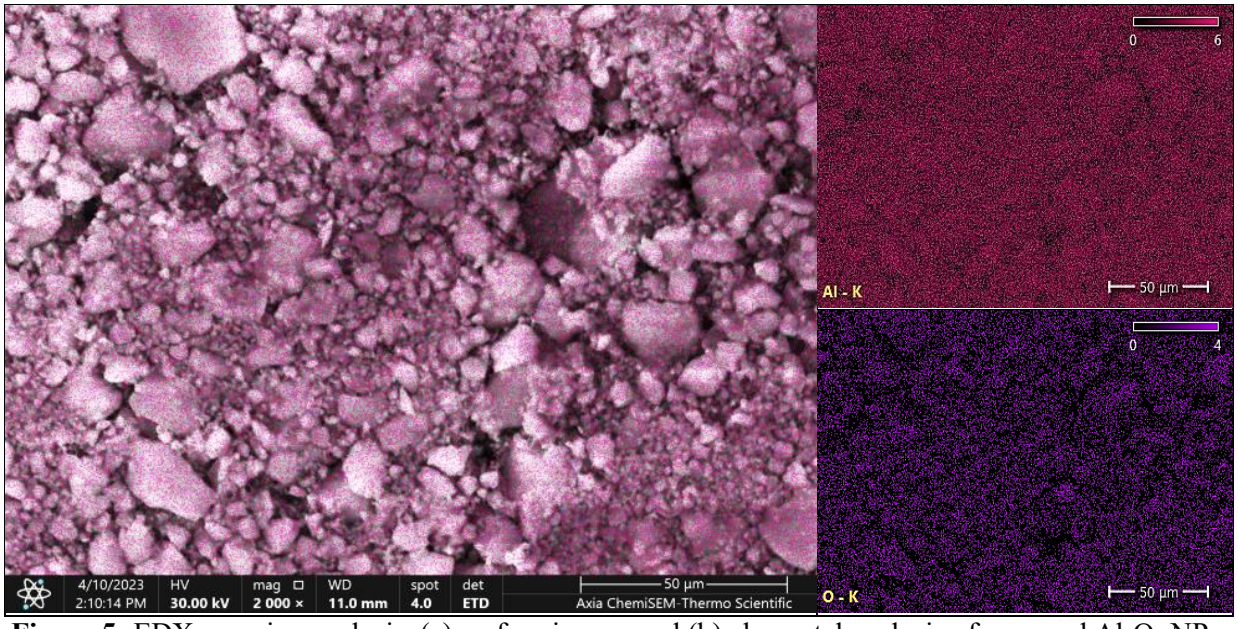

Figure 5: EDX mapping analysis, (a) surface image, and (b) elemental analysis of prepared Al_2O_3 NPs.

3.4 AFM Results

Fig. 6a and b shows AFM images (both 2D and 3D) with the average size histogram of the Al_2O_3 nanoparticles prepared in the current study. The high surface roughness of the prepared sample is essential for gamma shielding as a radiation-matter interaction application. The irregularity in topography and increase in surface roughness can result from a higher surface-to-volume ratio in the prepared material. Consequently, the grain size is reduced to below 100 nm; this surface-to-volume ratio can be significantly increased. According to the histogram in **Fig. 6c**, the most dominant grain sizes are below 50 nm, and the average grain size is 40.7 nm; therefore, it is evident that the prepared sample exhibits high surface roughness and surface-to-volume ratio [29].

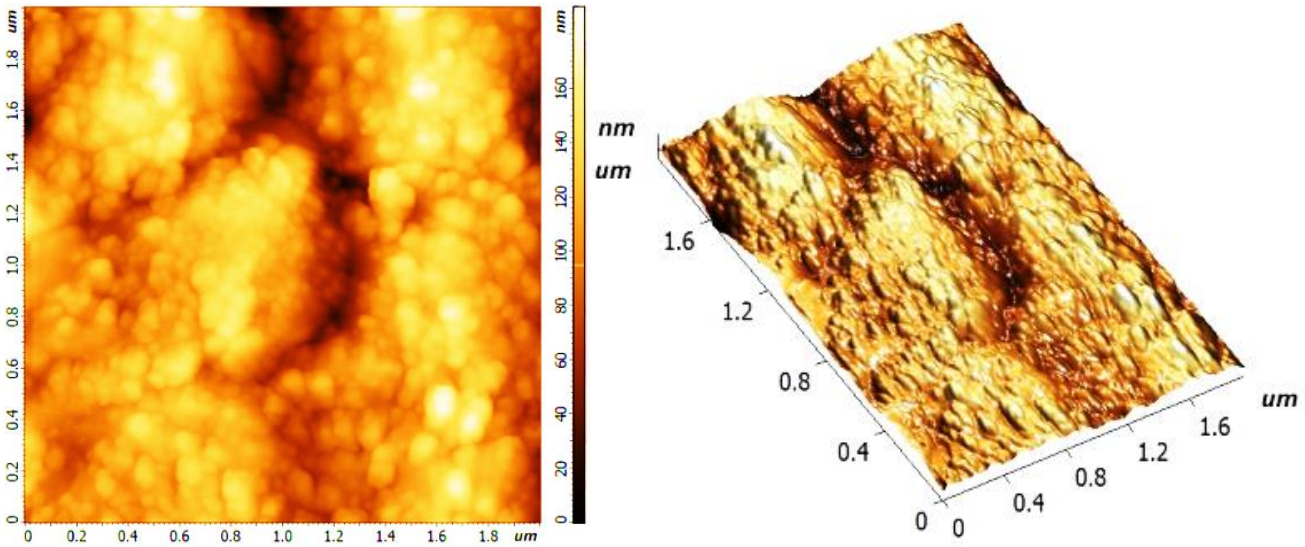

(a) (b)

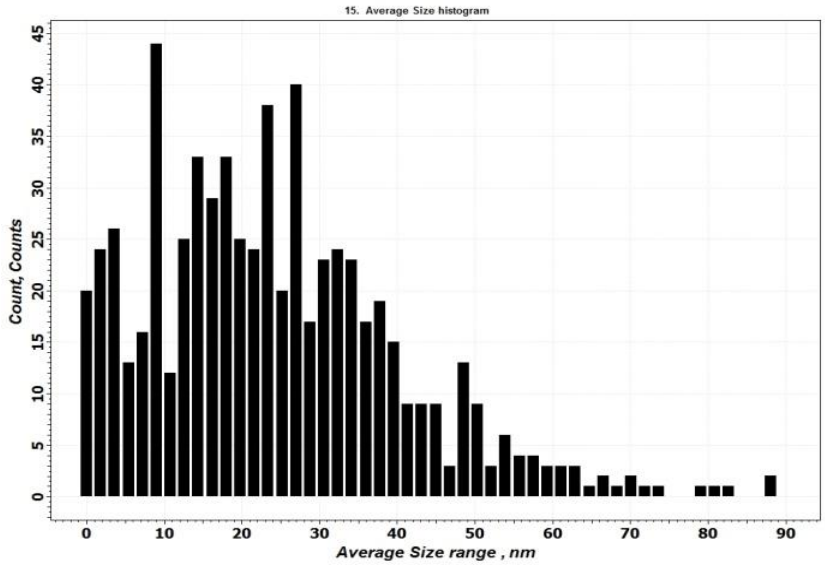

(c)

Figure 6: AFM images (a) 2D, (b) 3D, and (c) average size histogram of prepared Al_2O_3 NPs.

3.5 FTIR Results

Fig. 7 demonstrates the FTIR spectrum of the prepared Al_2O_3 nanoparticles. Principally, as a polyatomic molecule with 5 atoms, as shown in **Fig. 1**, there are 3N-5=10 vibration modes. Therefore, the distinct absorption peaks within the wave number range of 400 to 700 cm^{-1} are attributed to the vibration modes of the Al_2O_3 molecules. However, some peaks may be composed of two or more modes vibrating at the same wave number but with

perpendicular planes. The absorption peaks assigned at 406.69, 412.12, 420.03, 423.54, 431.30, 490.39, and 559.25 cm^{-1} due to stretching modes of the Al-O and Al=O bonds, while the absorption peak assigned at 634.09 cm^{-1} has resulted from the bending modes of the Al-O-Al bond, which confirms the formation of the gamma phase of alumina (γ-Al_2O_3). Consequently, the prepared Al_2O_3 phase contains the tetrahedral and octahedral coordination [49].

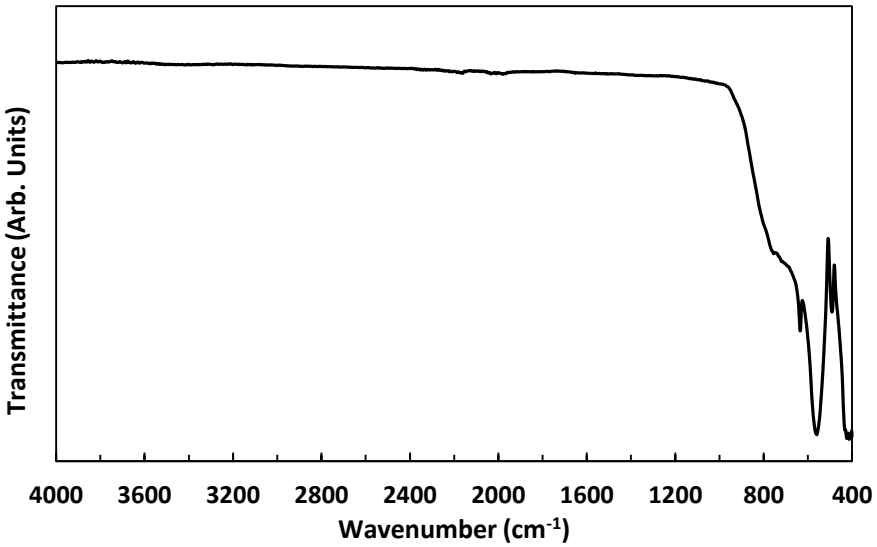

Figure 7: FTIR spectrum of prepared Al_2O_3 NPs.

All relatively weak absorption peaks at wave numbers higher than 1500 cm^{-1} are ascribed to the vibration modes of the O-H bond (stretching and bending) in the molecules of water adsorbed on the surface of the prepared nanoparticles from the surrounding environment [44]. Table 2 shows FTIR vibration modes of prepared Al_2O_3 NPs.

Table 2: Assignments of FTIR vibration modes of prepared Al_2O_3 NPs.

Bond	Wave number (cm^{-1})	Vibration mode
Al-O	406.69	Stretching
	412.12	Stretching
	420.03	Stretching
	423.54	Stretching
	431.30	Stretching
	490.39	Stretching
	559.25	Stretching
Al-O-Al	634.09	Bending

Fig. 8 shows the absorption spectrum of the prepared Al_2O_3 nanoparticles within the wavelength range of 200-1000 nm. The absorbance of this nanomaterial decreases with increasing wavelengths in the UV region and reaches its minimum at 250 nm. Then, the absorbance slightly increases to a maximum of 278 nm before decreasing continuously with wavelength. An absorption edge can be recognised at 278 nm, at which the energy band gap of the Al_2O_3 nanoparticles can be determined according to equation 1.24/Eg to be 4.46 eV, which is noticeably smaller than the typical values of the energy band gap of bulk γ-Al_2O_3 (7.0-8.7 eV) [50-52].

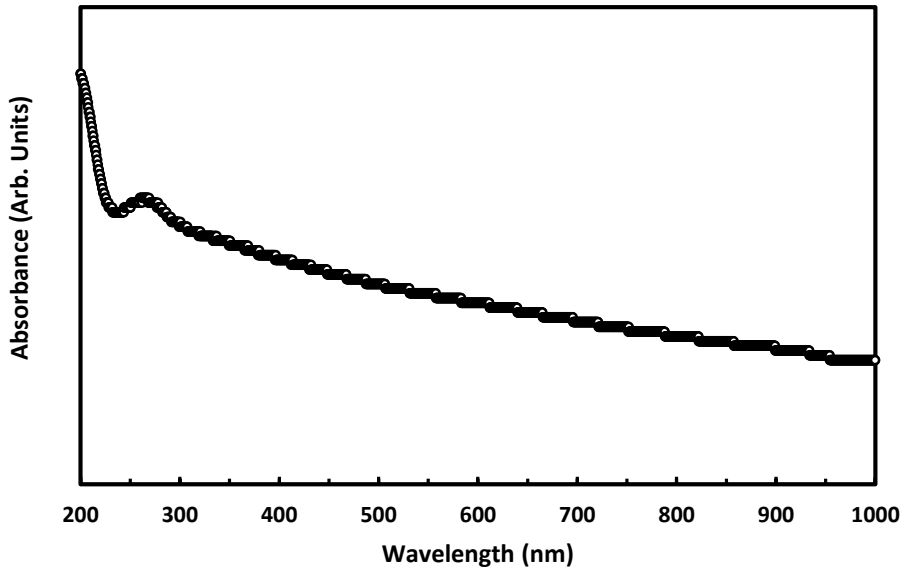

Figure 8: Absorption spectrum of the prepared Al_2O_3 nanoparticles.

4. Conclusions

In concluding remarks, the technique of DC reactive sputtering was employed to synthesize Al_2O_3 nanoparticles by sputtering an extremely pure aluminum target in the presence of oxygen in the gas mixture that contained Ar and O_2. The produced samples had an amorphous, polycrystalline structure because of the formation of nanoparticles, which had an average grain size of 40.7 nm and a minimum size of 21 nm, making them roughly spherical. The prepared material comprises oxygen and aluminum without trace amounts of other elements. Additionally, the stoichiometry and homogeneity of the obtained material were confirmed. It was confirmed that all functional groups corresponded to the vibrational modes of the Al_2O_3 molecule.

Conflict of Interest

The authors declare that they have no conflict of interest.

References

[1] A. M. El-Khatib, M. I. Abbas, M. A. Elzaher, M. S. Badawi, M. T. Alabsy, G. A. Alharshan, *et al.*, "Gamma attenuation coefficients of nano cadmium oxide/high density polyethylene composites," *Sci. Rep.*, vol. 9, no. 1, p. 16012, 2019.

[2] A. R. Pai, N. Puthiyaveettil Azeez, B. Thankan, N. Gopakumar, M. Jaroszewski, C. Paoloni, *et al.*, "Recent progress in electromagnetic interference shielding performance of porous polymer nanocomposites—a review," *Energies*, vol. 15, no. 11, p. 3901, 2022.

[3] A. Acevedo-Del-Castillo, E. Águila-Toledo, S. Maldonado-Magnere, and H. Aguilar-Bolados, "A brief review on the high-energy electromagnetic radiation-shielding materials based on polymer nanocomposites," *Int. J. Mol. Sci.*, vol. 22, no. 16, p. 9079, 2021.

[4] C. Liang, Z. Gu, Y. Zhang, Z. Ma, H. Qiu, and J. Gu, "Structural design strategies of polymer matrix composites for electromagnetic interference shielding: a review," *Nano-micro Lett.*, vol. 13, no. 1, p. 181, 2021.

[5] D. Jiang, V. Murugadoss, Y. Wang, J. Lin, T. Ding, Z. Wang, *et al.*, "Electromagnetic interference shielding polymers and nanocomposites-a review," *Polym. Rev.*, vol. 59, no. 2, pp. 280–337, 2019.

[6] M. I. Sayyed, H. O. Tekin, M. M. Taki, M. H. A. Mhareb, O. Agar, E. Şakar, *et al.*, "Bi_2O_3-B_2O_3-ZnO-BaO-Li_2O glass system for gamma ray shielding applications," *Optik (Stuttg).*, vol. 201, p. 163525, 2020.

[7] M. D. Hassib, K. M. Kaky, A. Kumar, E. Şakar, M. I. Sayyed, S.O. Baki *et al.*, "Boro-silicate glasses co-doped Er^{+3}/Yb^{+3} for optical amplifier and gamma radiation shielding applications," *Phys. B Condens. Matter*, vol. 567, pp. 37–44, 2019.

[8] D. Wanasinghe, F. Aslani, G. Ma, and D. Habibi, "Review of polymer composites with diverse nanofillers for electromagnetic interference shielding," *Nanomaterials*, vol. 10, no. 3, p. 541, 2020.

[9] E. Rajasekhar, K. L. Narasimham, A. D. Kurdekar, L. A. A. Chunduri, S. Parnaik, and K. Venkataramaniah, "Mass attenuation coefficient measurements of some nanocarbon allotropes: a new hope for better low cost less-cumbersome radiation shielding over a wide energy range," *J. Nucl. Physics, Mater. Sci. Radiat. Appl.*, vol. 5, no. 2, pp. 311–317, 2018.

[10] G. Angarita, C. Palacio, M. Trujillo, and M. Arroyave, "Synthesis of alumina thin films using reactive magnetron sputtering method," in *Journal of Physics: Conference Series*, IOP Publishing, 2017, p. 12022.

[11] G. Zhou, L. Wang, X. Wang, and Y. Yu, "Deposition of nanostructured crystalline alumina thin film by twin targets reactive high power impulse magnetron sputtering," *Appl. Surf. Sci.*, vol. 455, pp. 310–317, 2018.

[12] I. G. Alhindawy, M. I. Sayyed, A. H. Almuqrin, and K. A. Mahmoud, "Optimizing gamma radiation shielding with cobalt-titania hybrid nanomaterials," *Sci. Rep.*, vol. 13, no. 1, p. 8936, 2023.

[13] K. S. Kumar, R. Rengaraj, G. R. Venkatakrishnan, and A. Chandramohan, "Polymeric materials for electromagnetic shielding-A review," *Mater. Today Proc.*, vol. 47, pp. 4925–4928, 2021.

[14] Y. S. Rammah, K. A. Mahmoud, F. Q. Mohammed, M. I. Sayyed, O. L. Tashlykov, and R. El-Mallawany, "Gamma ray exposure buildup factor and shielding features for some binary alloys using MCNP-5 simulation code," *Nucl. Eng. Technol.*, vol. 53, no. 8, pp. 2661–2668, 2021.

[15] K. Shahapurkar, M. Gelaw, V. Tirth, M. E. M. Soudagar, P. Shahapurkar, M. A. Mujtaba, *et al.*, "Comprehensive review on polymer composites as electromagnetic interference shielding materials," *Polym. Polym. Compos.*, vol. 30, p. 09673911221102127, 2022.

[16] K. J. Singh, S. Kaur, and R. S. Kaundal, "Comparative study of gamma ray shielding and some properties of PbO–SiO_2–Al_2O_3 and Bi_2O_3–SiO_2–Al_2O_3 glass systems," *Radiat. Phys. Chem.*, vol. 96, pp. 153–157, 2014.

[17] L. Omana, A. Chandran, R. E. John, R. Wilson, K. C. George, N. V. Unnikrishnan, *et al.*, "Recent advances in polymer nanocomposites for electromagnetic interference shielding: a review," *ACS omega*, vol. 7, no. 30, pp. 25921–25947, 2022.

[18] M. Elsafi, A. H. Almuqrin, H. M. Almutairi, W. M. Al-Saleh, and M. I. Sayyed, "Grafting red clay with Bi2O3 nanoparticles into epoxy resin for gamma-ray shielding applications," *Sci. Rep.*, vol. 13, no. 1, p. 5472, 2023.

[19] M. Nadeem, M. Mehrban, M. A. Javid, and M. A. Saeed, "Development of electromagnetic interference shielding materials over time: A review," *Int J Nanoelectron Mater*, vol. 14, no. 1, pp. 71–98, 2021.

[20] J. Wang, D. Li, Q. Liu, X. Yin, Y. Zhang, X. Jing, *et al.*, "Fabrication of hydrophobic surface with hierarchical structure on Mg alloy and its corrosion resistance," *Electrochim. Acta*, vol. 55, no. 22, pp. 6897–6906, 2010.

[21] J. K. Oleiwi, M. S. Hamza, and M. S. Abed, "A study of the hardness and wear rate of elastomer composites reinforced by Al_2O_3 and SiO_2 particles," *Eng. Technol. J.*, vol. 27, no. 7, pp. 1423–1434, 2009.

[22] R. A. Anaee, "Alumina Nanoparticle/Polypyrrole Coating for Carbon Steel Protection in Simulated Soil Solution," *Eng. Technol. J.*, vol. 35, no. 9 Part A, 2017.

[23] N. C. for B. Information, "PubChem compound summary." National Center for Biotechnology Information Bethesda, MD, USA, 2021.

[24] M. I. Abbas, A. M. El-Khatib, M. Elsafi, S. N. El-Shimy, M. F. Dib, H. M. Abdellatif, *et al.*, "Investigation of gamma-ray shielding properties of bismuth oxide nanoparticles with a bentonite–gypsum matrix," *Materials (Basel).*, vol. 16, no. 5, p. 2056, 2023.

[25] M. M. Gouda, A. M. El-Khatib, M. M. Khalil, M. Abd-Elzaher, and M. I. Abbas, "Comparative study between micro-and nano-carbon with epoxy for gamma shielding applications," *Carbon Lett.*, vol. 34, no. 4, pp. 1129–1141, 2024.

[26] M. T. Alabsy, M. M. Gouda, M. I. Abbas, S. M. Al-Balawi, and A. M. El-Khatib, "Enhancing the gamma-radiation-shielding properties of gypsum–lime–waste marble mortars by incorporating micro-and nano-PbO particles," *Materials (Basel).*, vol. 16, no. 4, p. 1577, 2023.

[27] N. Zaım and O. Bayhatun, "A Study on the Gamma-Ray Attenuation Coefficients of Al_2O_3 and Al_2O_3. TiO_2 Compounds," *Süleyman Demirel Üniversitesi Fen Bilim. Enstitüsü Derg.*, vol. 22, pp. 312–318, 2018.

[28] N. A. Kawady, M. Elkattan, M. Salah, and A. A. Galhoum, "Fabrication, characterization, and gamma ray

shielding properties of PVA-based polymer nanocomposite," *J. Mater. Sci.*, vol. 57, no. 24, pp. 11046–11061, 2022.

[29] R. A. Ismail, K. S. Khashan, and A. M. Alwan, "Study of the effect of incorporation of CdS nanoparticles on the porous silicon photodetector," *Silicon*, vol. 9, pp. 321–326, 2017.

[30] F. Shivanand, "Magdaline Eljeeva Emerald and Somveer,"Synthesis and characterization of aluminum oxide nanoparticles," *Pharma Innov. J.*, vol. 11, no. 6, pp. 1068–1072, 2022.

[31] R. A. Issa, M. N. Al-Shroofy, and H. A. Al-Kaisy, "Al_2O_3-TiO_2-PMMA bio-composite coating via electrostatic spray technique," *Eng. Technol. J.*, vol. 39, no. 3A, pp. 504–511, 2021.

[32] S. U. Ilyas, R. Pendyala, and N. Marneni, "Stability and agglomeration of alumina nanoparticles in ethanol-water mixtures," *Procedia Eng.*, vol. 148, pp. 290–297, 2016.

[33] A. J. Owaid, "Characterization of AA 6061–alloy composites reinforced by Al_2O_3 nano particles obtained by stir casting," *Eng. Technol. J.*, vol. 36, no. 7 Part A, 2018.

[34] B. T. Chiad, O. A. Hammadi, F. J. Kadhim, and M. K. Khalaf, "Langmuir Probe Diagnostics of Low-Pressure Glow Discharge Plasma Using Argon-Nitrogen Mixtures," *Iraqi J. Appl. Phys.*, vol. 12, no. 3, 2016.

[35] V. F. Nunes, P. H. F. M. Júnior, A. F. L. Almeida, and F. N. A. Freire, "Surface properties of Al2O3: ZnO thin films growth on FTO for photovoltaic application," *Next Mater.*, vol. 2, p. 100069, 2024.

[36] H. H. Lemago, N. Khauli, D. Hessz, T. Igricz, P. Petra, C. Cserháti, *et al.*, "Fabrication of ZnO–Al2O3 inverse opals with atomic layer deposited Amorphous-Al_2O_3 for enhanced photocatalysis," *Mater. Sci. Semicond. Process.*, vol. 183, p. 108733, 2024.

[37] S. J. Park, Y. Y. Choi, J. G. Kim, and D. J. Choi, "Growth and mechanism of one-dimensional Al_2O_3 nanostructures grown by chemical vapor deposition from an Al powder source," *J. Cryst. Growth*, vol. 361, pp. 189–194, 2012.

[38] G. E. Stan, M. Montazerian, A. Shearer, B. W. Stuart, F. Baino, J. C. Mauro, *et al.*, "Critical advances in the field of magnetron sputtered bioactive glass thin-films: An analytical review," *Appl. Surf. Sci.*, vol. 646, p. 158760, 2024.

[39] F. Delkhosh, A. Qotbi, A. H. Behroozi, and V. Vatanpour, "Magnetron sputtering in membrane fabrication and modification: Applications in gas and water treatment," *J. Ind. Eng. Chem.*, 2024.

[40] R. Garg, S. Gonuguntla, S. Sk, M. S. Iqbal, A. O. Dada, U. Pal, *et al.*, "Sputtering thin films: Materials, applications, challenges and future directions," *Adv. Colloid Interface Sci.*, p. 103203, 2024.

[41] H. Larhlimi, A. Ghailane, M. Makha, and J. Alami, "Magnetron sputtered titanium carbide-based coatings: A review of science and technology," *Vacuum*, vol. 197, p. 110853, 2022.

[42] C. Fernández-González, S. Ruiz-Gómez, A. Arché-Núñez, L. Pérez, and C. T. de Sousa, "Nano-patterning using ultra-thin alumina membranes," *Mater. Today Nano*, p. 100553, 2024.

[43] M. A. Hameed, S. H. Faisal, and R. H. Turki, "Characterization of Multilayer Highly-Pure Metal Oxide Structures Prepared by DC Reactive Magnetron Sputtering," *IRAQI J. Mater.*, vol. 3, no. 4, pp. 1–8, 2024.

[44] A. M. Hameed and M. A. Hameed, "Highly-pure nanostructured metal oxide multilayer structure prepared by DC reactive magnetron sputtering technique," *Iraqi J. Appl. Phys.*, vol. 18, no. 4, 2022.

[45] O. A. Hammadi, "Production of nanopowders from physical vapor deposited films on nonmetallic substrates by conjunctional freezing-assisted ultrasonic extraction method," *Proc. Inst. Mech. Eng. Part N J. Nanomater. Nanoeng. Nanosyst.*, vol. 232, no. 4, pp. 135–140, 2018.

[46] O. A. Hammadi, "Effects of Extraction Parameters on Particle Size of Iron Oxide Nanopowders Prepared by Physical Vapor Deposition Technique," *Iraqi J. Appl. Phys.*, vol. 20, no. 2B, pp. 457–460, 2024.

[47] Y. Waseda, E. Matsubara, and K. Shinoda, *X-ray diffraction crystallography: introduction, examples and solved problems*. Springer Science & Business Media, 2011.

[48] H. E. Swanson, *Standard X-ray diffraction powder patterns*, vol. 25. US Department of Commerce, National Bureau of Standards, 1955.

[49] P. R. Griffiths, "Fourier transform infrared spectrometry," *Science (80-.).*, vol. 222, no. 4621, pp. 297–302, 1983.

[50] E. O. Filatova and A. S. Konashuk, "Interpretation of the changing the band gap of Al_2O_3 depending on its crystalline form: connection with different local symmetries," *J. Phys. Chem. C*, vol. 119, no. 35, pp. 20755–20761, 2015.

[51] S. I. Al-nassar, A. KM, and Z. F. Mahdi, "Study the effect of different liquid media on the synthesis of

alumina (Al_2O_3) nanoparticle by pulsed laser ablation technique," *Manuf Sci Technol*, vol. 3, pp. 77–81, 2015.

[52] S. Kaniyarakkal, T. Thomas, S. K. Sadagopalan, L. Jayamohan, R. Muralimanohar, L. Vasanthakumaryamma *et al.*, "Synthesis, linear and nonlinear optical properties of Ag/Al_2O_3 nanocomposites," *Materials (Basel).*, vol. 15, no. 18, p. 6322, 2022.